Journal of Hydroscience and Hydraulic Engineering
Vol. 28, No.2 November, 2010, 49-64

NUMERICAL PREDICTION FOR MOVEMENTS OF A FLOATING OBJECT WITH NON-UNIFORM DENSITY IN FREE SURFACE FLOWS

By

Satoru Ushijima

ACCMS, Kyoto University, Kyoto-shi, 606-8501, Japan

Nozomu Kuroda

CERE, Kyoto University, Kyoto-shi, 615-8540, Japan

and

Genta Nakamura

CERE, Kyoto University, Kyoto-shi, 615-8540, Japan

SYNOPSIS

This paper deals with a computational method to predict the motions of floating objects which have density distributions in free-surface flows. The density distribution of the floating object is taken into account in the prediction method, since it is closely related to the stability of the initial attitude and its motion. The motions of the floating object and free-surface flows are simultaneously dealt with in the computational method, MICS (Multiphase Incompressible flow solver with Collocated grid System), which enables us to deal with the multiphase field consisting of gas, liquid and solid phases. The floating object is represented by multiple tetrahedron elements with different density one by one, from which the volume-averaged density of a fluid cell is determined through a sub-cell method. The prediction method was applied to the movements of a floating cylinder with non-uniform density and mangrove propagule. As a result of the computations, it was demonstrated that the basic features of their motions are reasonably predicted through the comparison with the experimental results.

INTRODUCTION

It is an important subject in hydraulic engineerings to predict the behaviors of floating structures and objects in free-surface flows. In particular, it is necessary to take into account the density distributions within an object itself as well as the its global shape and mean density, when evaluating its stable attitude and response against free-surface oscillations and fluid flows. One of the interesting examples of floating bodies can be found in the mangrove propagules, which are transported in coastal currents and their floating attitudes are closely related to geographical distributions. For example, the propagule of *Bruguiera gymnorrhiza* floating in water is shown in Fig. 1. The vertical attitudes, their axial density distributions and the depth in water are mutually related to determine their zonation in waterfront regions. In addition, it has been reported that the attitude depends on the inside structures of the propagule, especially on its density distribution (1).

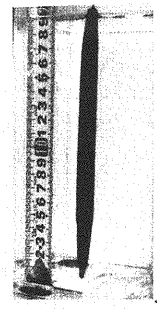

Fig. 1 Mangrove propagule floating in water tank

In this paper, a computational method is investigated to predict the attitude and movement of the floating object with density distribution. In the previous studies regarding floating objects in waves, the assumption of potential flow was employed in many cases (2). In contrast to them, in the present computational method, this assumption is discarded and the interactions between fluid flows and the behaviors of floating objects are directly evaluated with a multiphase modeling, MICS (Multiphase Incompressible flow solver with Collocated grid System) (3). While in our previous studies the objects in flows have uniform density (4), the density distribution is taken into account in the present study by setting independently the densities of multiple tetrahedron elements consisting of an object.

In order to confirm the validity of the proposed computational method, it was applied to the movements of a cylinder consisting of two parts which have different densities and to the behaviors of an actual mangrove propagule in a water tank. The computational results were compared with the experimental results.

NUMERICAL PROCEDURES

Computational method for floating bodies in free-surface flows

The computational method for multiphase fields, MICS (5) is used to deal with the movement of floating bodies in free-surface flows. As shown in our previous paper (3), first the multiphase fields consisting of gas and liquid phases are solved. Then the fluid forces acting on solid objects are evaluated by means of the obtained computational results by taking account of the densities of the objects. The governing equations, which correspond to those of one-fluid modeling, for gas and liquid phases are given by

$$\frac{\partial \rho_f}{\partial t} + \frac{\partial}{\partial x_j}(\rho_f u_j) = 0 \tag{1}$$

$$\frac{\partial u_j}{\partial x_j} = 0 \tag{2}$$

$$\frac{\partial u_i}{\partial t} + \frac{\partial}{\partial x_j}(u_i u_j) = f_i - \frac{1}{\rho_f}\frac{\partial p}{\partial x_i} + \frac{1}{\rho_f}\frac{\partial}{\partial x_j}\left[\frac{\partial}{\partial x_j}(\mu u_i) + \frac{\partial}{\partial x_i}(\mu u_j)\right] \tag{3}$$

where t is time, x_i orthogonal coordinates, u_i mass-averaged velocity components of gas and liquid phases and f_i external acceleration component. The variables p, ρ_f and μ are volume-averaged pressure, density and viscous coefficient, respectively.

The governing equations are discretized in the collocated grid system which are fixed in the space on the basis of the finite volume method. The free-surface profiles are calculated by solving Eq. 1 with conservative

scheme. The fifth-order TVD scheme (6) is employed to solve the convective terms in the governing equations. The SMAC method is used to solve the equation system consisting of Eqs. 2 and 3. In the estimation stage, an implicit method, C-ISMAC (7), is used to solve the convective and diffusive equations. On the other hand, in the pressure computation stage, the C-HSMAC method (8) is applied to pressure Poisson equations, which enables us to obtain the pressure and velocity fields that satisfy incompressible conditions accurately.

Fluid forces acting on solid objects

When a part of a solid object is included in a computational fluid cell, the following equation, which corresponds to Eq. 3, is established:

$$\rho_b \frac{Du_i}{Dt} = -\rho_b g \delta_{3,i} - \frac{\partial p}{\partial x_i} + \frac{\partial}{\partial x_j}\left[\frac{\partial}{\partial x_j}(\mu u_i) + \frac{\partial}{\partial x_i}(\mu u_j)\right] \tag{4}$$

where g is gravity acceleration, x_3 vertical coordinate in upward direction and $\delta_{i,j}$ Kronecker's delta. The variable ρ_b is the density evaluated with the mass of the solid object that occupies in a fluid cell and its value is determined by means of the sub-cell method described in the following section. The sub-cells are created by dividing one fluid cell into smaller ones. The sub-cell method allows us to evaluate the volume of a part of the solid phase included in a fluid cell by counting the number of sub-cells within the solid area.

The pressure p^{n+1}, which is obtained after pressure computation, is defined as $p^{n+1} = p_0 + \phi^*$, where p_0 is the hydrostatic pressure and ϕ^* is the pressure deviation from p_0. The Eq. 4 can be written with this expression as

$$\frac{Du_i}{Dt} = -\frac{\rho_b - \rho_f}{\rho_b} g \delta_{3,i} - \frac{1}{\rho_b}\frac{\partial \phi^*}{\partial x_i} + \frac{1}{\rho_b}\frac{\partial}{\partial x_j}\left[\frac{\partial}{\partial x_j}(\mu u_i) + \frac{\partial}{\partial x_i}(\mu u_j)\right] \tag{5}$$

The first, second and third terms on the right hand side of Eq. 5 correspond to the buoyancy, dynamic pressure and viscous terms respectively.

The fluid forces acting on solid objects can be determined from the right hand side of Eq. 5. The fluid force component, F_{Ci}, acting on a part of the solid object in a fluid cell C is calculated with the following relationship:

$$F_{Ci} = \alpha \rho_b V_C \cdot RHS \tag{6}$$

where V_C is the volume of a fluid cell, α is the volume fraction of the solid phase in the cell and RHS stands for the right hand side of Eq. 5.

Treatment of floating body having density distribution

Fig. 2 shows the two-dimensional schematic view of the relationship among a fluid cell, sub-cells and the tetrahedron elements.

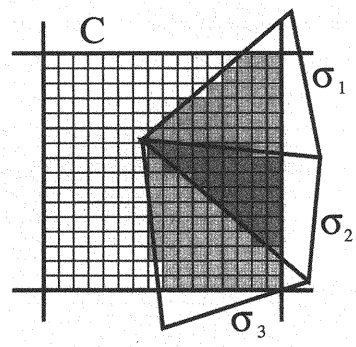

Fig. 2 Relationship among fluid cell (thick lines), sub-cells (thin lines) and tetrahedron elements (triangles)

While the density of each element is uniform, the density distribution in the solid object can be represented by setting different densities for the multiple elements belonging to it independently. After the volume fraction γ_i of an element i included in the fluid cell C is determined by the sub-cell numbers, the volume-averaged density of the fluid cell ρ_b is calculated by means of the following equation:

$$\rho_b = \rho_f \left(1 - \sum_i \gamma_i\right) + \sum_i \gamma_i \sigma_i \tag{7}$$

where ρ_f is the density of the gas and liquid phases, while σ_i is the density of the element i for a solid object.

COMPUTATIONS OF CYLINDRICAL OBJECT

Basic properties of cylinder with density distribution

In this section, as shown in Fig. 3, the basic behaviors of the cylindrical object which consists of two cylinders with different densities are investigated.

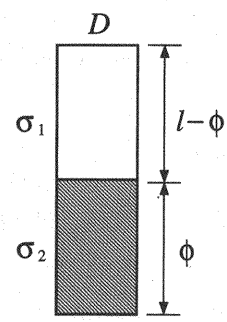

Fig. 3 Cylinder consisting of two parts with different densities

The densities and the lengths of the upper and lower cylinders are σ_1, σ_2, $l-\phi$ and ϕ, respectively, as shown in Fig. 3. The densities of water and air are denoted by ρ_w and ρ_a respectively, where it is approximated that $\rho_a \approx 0$. The densities σ_1, σ_2 are satisfied the following condition:

$$\sigma_2 > \rho_w > \sigma_1 \tag{8}$$

The attitude of the cylindrical object with neutral buoyancy in water is shown in Fig. 4. As shown in Fig. 4, the z' is set in the vertical upward direction with its origin on the bottom of the cylinder. The points, where gravity and buoyancy forces act, are denoted as G and B, respectively, and their heights are given by z_b and z_g. The distance between the bottom surface of the cylinder and the water surface is defined as h_b.

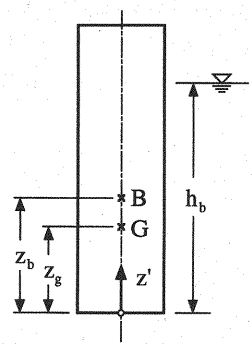

Fig. 4 Cylindrical object in neutral buoyancy and z' coordinate

Since the cylindrical object floats on the water surface, the following conditions must be established:

$$a \equiv \frac{\rho_w - \sigma_1}{\sigma_2 - \sigma_1} - \frac{\phi}{l} > 0 \tag{9}$$

The distances z_b and z_g are given by

$$z_b = \frac{1}{2}\frac{\sigma_1 l + (\sigma_2 - \sigma_1)\phi}{\rho_w} \tag{10}$$

and

$$z_g = \frac{1}{2}\frac{(\sigma_2 - \sigma_1)\,\phi^2 + \sigma_1 l^2}{\sigma_1 l + (\sigma_2 - \sigma_1)\phi} \tag{11}$$

where $h_b = 2z_b$. In addition, to keep the stable attitude as shown in Fig. 4, the following relationship needs to be satisfied:

$$b \equiv \frac{D^2}{16l}\frac{\rho_w}{\sigma_1 l + (\sigma_2 - \sigma_1)\phi} + \frac{z_b - z_g}{l} > 0 \tag{12}$$

On the other hand, the rotating motion is considered around horizontal axis H from the neutral attitude. Assuming that the rotating angle is sufficiently small and that the height of the axis H from the bottom of the cylinder is given by z_c, the moment of inertia I around axis H is given as follows with the parallel axis theorem:

$$I = \frac{\pi D^2 \sigma_2}{4}\int_0^{\phi}\left[\frac{D^2}{16} + (z' - z_c)^2\right]dz' + \frac{\pi D^2 \sigma_1}{4}\int_{\phi}^{l}\left[\frac{D^2}{16} + (z' - z_c)^2\right]dz' \tag{13}$$

The angular momentum equation can be written with the couple of gravity and buoyancy forces N and a sufficiently small angle θ as

$$I\ddot{\theta} = N \tag{14}$$

It can be approximated that $N \approx MgL\theta$, where g is gravity acceleration and L is the distance between metacenter and G. Thus the time period of rotating oscillation is given by

$$T = 2\pi\sqrt{\frac{I}{MgL}} \tag{15}$$

Experiments using cylinder with density distribution

The movements of the cylindrical object consisting of two parts having different densities were measured in the experiments, in order to understand its actual behaviors. The cylindrical object used in the experiments is made of wood and acrylic cylinder parts with the densities of $\sigma_1/\rho_w = 0.5$ and $\sigma_2/\rho_w = 1.18$. The axial lengths are $l = 0.1$ m and $D = 30$ mm. Fig. 5 shows the values of a and b calculated in Eqs. 9 and 12 against ϕ/l. Both a and b must be positive so that the cylindrical object can float in the attitude as shown in Fig. 4. This condition is satisfied in the range of $\phi_1' < \phi/l < \phi_2'$, where $\phi_1' \approx 0.4$ and $\phi_2' \approx 0.73$. Taking account of the above conditions, ϕ/l is set at 0.5, 0.6 ,0.7 in the experiments.

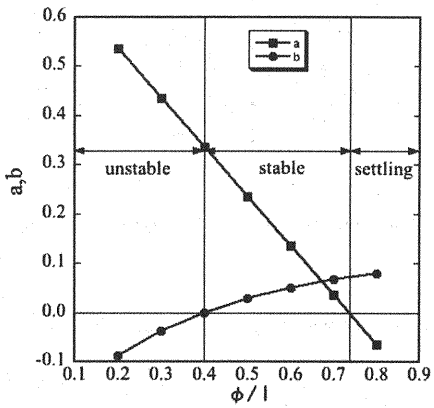

Fig. 5 Relationship between a, b and ϕ/l

Two types of experiments were conducted: case-A and case-B. In case-A, free oscillations of the cylindrical object were captured through a video camera by setting the initial central axis inclined by about 14 degrees against the vertical axis. On the other hand, in case-B, the water tank of 0.19 m × 0.06 m × 0.2 m including the floating cylinder is accelerated to cause the first-order sloshing motions of the free surface. The floating object in neutral buoyancy in the initial water depth of 0.15 m was forced to move by the sloshing. After an acceleration of 1.0 m/s^2 was imposed for 0.224 sec., the negative acceleration of -1.0 m/s^2 was added during the same period of time. The value ϕ/l of the cylindrical object was fixed at 0.6 in case-B.

Computations of cylinder regarding stability of initial attitudes

In the computations, fluid cells with 5 × 5 × 5 mm were set up for air and water regions. The cell number was 38 × 12 × 40. The cylindrical object was represented by multiple tetrahedron elements as shown in Fig. 6. The total numbers of elements and nodes were 1,471 and 436 respectively.

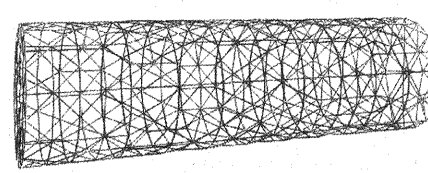

Fig. 6 Cylindrical model and its elements used in computations

In the computations, the following conditions were employed: The density and viscous coefficients of water are 1.0 $\times 10^3$ kg/m^3 and 1.0 $\times$ 10^{-6} m^2/s respectively, while these values for air are 1.0 kg/m^3 and 1.0 $\times$ 10^{-5} m^2/s respectively.

First, the stability of the initial attitude of the cylindrical object is examined in the computation. Fig. 7 shows the predicted behaviors of the cylinder with $\phi/l = 0.35$, which is theoretically in the unstable condition as shown in Fig. 5. As shown in Fig. 7, it is reasonably predicted that the initial attitude, in which the center axis of the cylinder is parallel with the vertical direction, is unstable and that the transition from the initial attitude to the horizontal one.

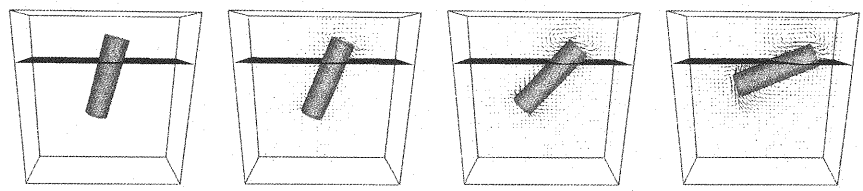

(a) $t = 0.0$ (s) (b) $t = 0.2$ (s) (c) $t = 0.4$ (s) (d) $t = 0.6$ (s)

Fig. 7 Predicted results for unstable conditions ($\phi/l = 0.35$)

On the other hand, the cylindrical object falls in the water with the condition $\phi_2' < \phi$. To confirm this fact, the present computational method was applied to the cylinder with $\phi/l = 0.75$. As shown in Fig. 8, the falling process with oscillating motions of the cylinder is successfully predicted.

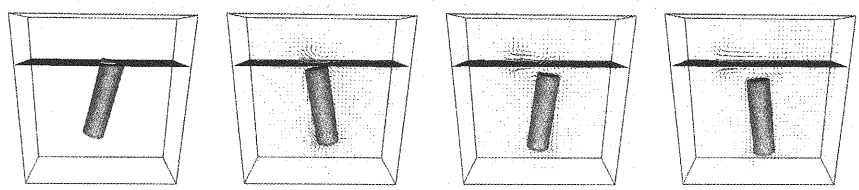

(a) $t = 0.0$ (s) (b) $t = 0.5$ (s) (c) $t = 1.0$ (s) (d) $t = 1.5$ (s)

Fig. 8 Predicted results for sinking cylinder ($\phi/l = 0.75$)

In addition, it was confirmed that the predicted initial attitude is stable in the condition of $0.5 \leq \phi \leq 0.7$ as theoretically shown in Fig. 5. In conclusion, the present computational method allows us to predict suitably the stability of the initial attitude of the cylindrical object with density distribution.

Computations of free oscillation of cylinder

The free oscillations of the cylindrical object with density distribution were calculated for the conditions of $\phi/l = 0.5,\ 0.6,\ 0.7$. The initial attitude of the cylinder was set so that the angle between its central axis and vertical axis is 14 degrees and the cylinder has neutral buoyancy. The cylinder was released from the initial position and the oscillating motions were numerically predicted. Fig. 9 shows the predicted results for the cylinder

of $\phi/l = 0.5$. As shown in Fig. 9, the cylinder shows rotational oscillations around the horizontal axis near the center point, which decrease due to the viscous effects of the surrounding fluid.

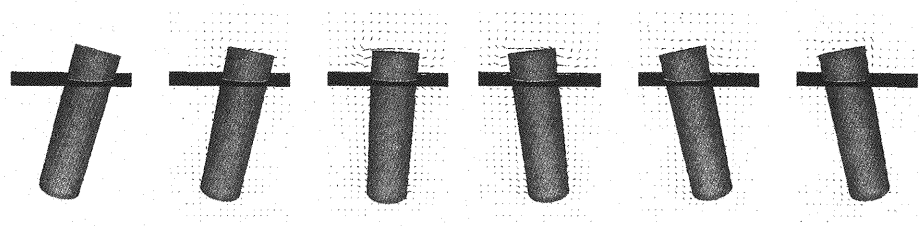

(a) $t = 0.0$ (s) (b) $t = 0.2$ (s) (c) $t = 0.4$ (s) (d) $t = 0.6$ (s) (e) $t = 0.8$ (s) (f) $t = 1.0$ (s)

Fig. 9 Predicted results for free oscillation ($\phi/l = 0.5$)

Fig. 10 shows the comparisons of time period T of free oscillation between experiments and computations. The lines in Fig. 10 are theoretical values obtained from Eq. 15, in which the lines A and B are derived when z_c is set at G and the center of free-surface level, respectively. As shown in Fig. 10, T decreases in the increase of ϕ and the experimental results are close to the line B. While the predicted results are somewhat larger than the experimental ones, their agreements are thought to be acceptable.

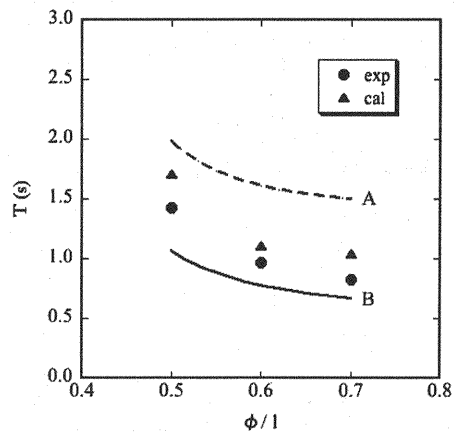

Fig. 10 Comparison of time period in free oscillations

Computations of cylinder motions in sloshing

The motions of cylindrical objects caused by free-surface sloshing were captured in the experiments by accelerating a water tank in which the cylindrical object of $\phi/l = 0.6$ is floating on the free-surface. As a result, a first-mode sloshing with a time period of about 0.5 sec. occurred in the tank. The time period of the sloshing is about half of the time period of natural oscillation of the cylinder.

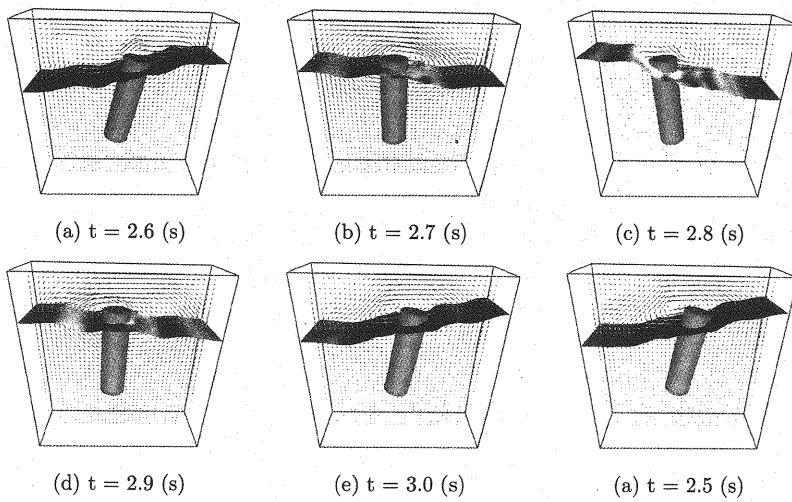

Fig. 11 Predicted results for cylinder motions in sloshing ($\phi/l = 0.6$)

Fig. 11 shows the predicted results for the motions of cylindrical object in sloshing flows. As shown in these results, the cylinder shows the rotating motions according to the free-surfaces oscillations around the horizontal axis near its bottom surface. This behavior agrees well with the experimental observations.

Fig. 12 shows the time history of the angle θ between the vertical axis and the central axis of the cylinder. The predicted results are shown in Fig. 12 with the experimental values. As shown in Fig. 12, it can be seen that they are generally in good agreement after 1.5 sec., while some discrepancies are found in the initial motion just after the acceleration is imposed.

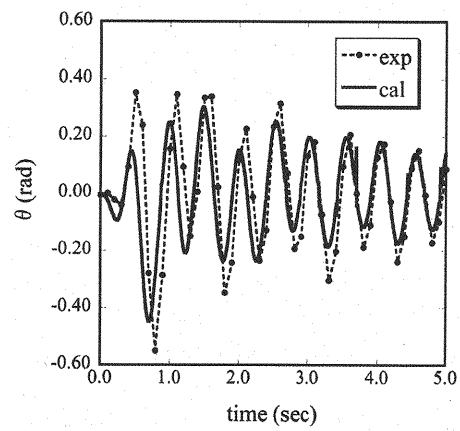

Fig. 12 Time history of θ in sloshing motions

Density distributions of actual mangrove propagule

Several mangrove propagules of *Bruguiera gymnorrhiza* were sampled in the actual field around Amami-Oshima in Japan to measure their axial density distributions and other properties. While there are somewhat differences among them, the average mass, volume and axial length L of the typical ones are 18.6 g, 18.9 cm^3 and 18.8 cm, respectively. The axial density distributions were investigated by cutting them into round slices and by measuring their mass and volume. Fig. 13 shows the relationship between specific density ρ_m and the normalized axial length z' measuring from the bottom of the propagules in the stable attitudes. As shown in Fig. 13, it was confirmed that the lower parts of the propagules have larger density than their upper areas and that it can be approximated based on the following linear relationship:

$$\rho_m = 1.11 - 0.256\ z' \tag{16}$$

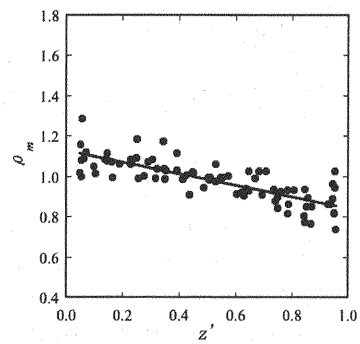

Fig. 13 Axial distributions of specific gravity in mangrove propagules

Hereafter, numerical predictions were conducted for the movements of a mangrove propagule of *Bruguiera gymnorrhiza*, which has the averaged shape as described above and is represented with the tetrahedron elements similarly to those shown in Fig. 6. The total numbers of elements and node points are 593 and 197 respectively. The axial density distributions are basically given by Eq. 16.

Computation of uniform density propagule

First of all, in order to confirm that the density distribution in mangrove propagule is essential to maintain its vertical attitude in free-surface flows, computations were performed in the artificial condition with uniform specific density, 0.978, which corresponds to the averaged value for a whole propagule. As shown in Fig. 14, it can be seen that the initial vertical attitude is unstable and that the propagule model with uniform density upsets to horizontal attitude. Thus, it is concluded that the density distribution of a propagule plays an important role in maintaining its vertical attitude in free-surface flows and that this situation can be properly treated by applying the present method.

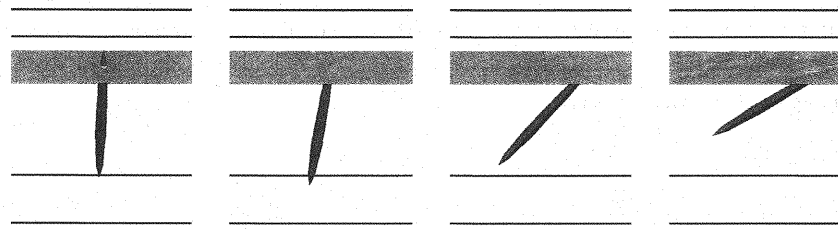

(a) $t = 0.0$ (s) (b) $t = 0.4$ (s) (c) $t = 0.8$ (s) (d) $t = 1.2$ (s)

Fig. 14 Predicted results of the mangrove propagule model having uniform density

Vertical free oscillation of mangrove propagule

The present computational method was applied to the vertical free oscillations of a propagule, in which its density distribution is taken into account. In both experiments and computations, one propagule was put in a rectangular water tank of 300 mm in length, 170 mm in width and 250 mm in height and the initial water depth was 200 mm. The center of gravity of the propagule was initially set at about 10 mm below the neutral position and then it was released to oscillate in a vertical direction on the free-surface. In the computations, fluid cells with $5 \times 5 \times 5$ mm are set up for air and water regions.

Fig. 15 shows the time history for the vertical displacements z from the neutral position of the propagule. As shown in Fig. 15, it can be seen that the mangrove propagule is oscillating periodically and the oscillations decrease due to the viscous effects of the surrounding fluid. It was shown that the natural period, around 1.5 sec., could be reasonably predicted by means of the present computational method.

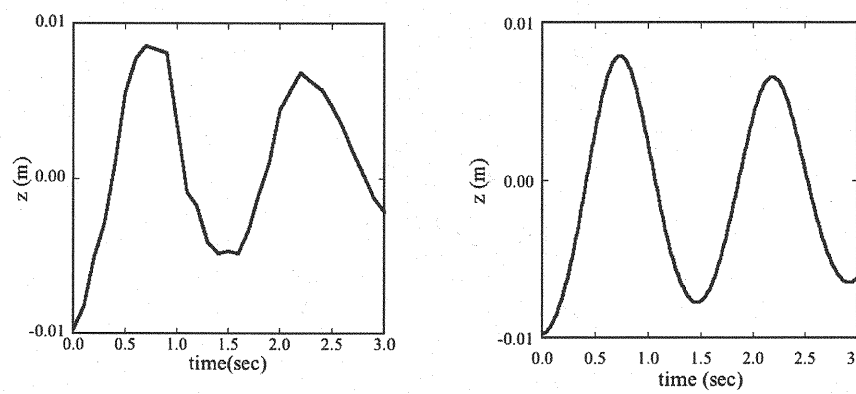

(a) Experiment (b) Calculation

Fig. 15 Time histories of vertical displacements in natural oscillation

Rotational movements of bended mangrove propagule

In this section, the rotational motions of a propagule are numerically investigated. While the central axis

of a mangrove propagule was assumed to be straight in calculations so far, the axis of the numerical model was artificially bent so that the maximum deformation vertical to its central axis is around 0.1 L in an attempt to simulate the actual propagules. Two types of propagules are shown in Fig. 16, which are a normal propagule with straight central axis and one which is bent.

(a) straight model (b) bent model

Fig. 16 Two types of numerical models for propagule

Three cases of calculations, case-A, B and C, were carried out with different initial attitudes and different models. In case-A, the straight model shown in Fig. 16 (a) is employed, while the bent model shown in Fig. 16 (b) is used for case-B and C. As schematically shown in Fig. 17, the basic attitude were firstly decided before setting the initial attitude; the central axis coincides with the vertical z axis in case-A, and the bent directions in case-B and C are set in $-x$ and $+y$ directions respectively. The initial attitude for computations were then determined by rotating them from the basic attitude by 14 degrees around the y axis.

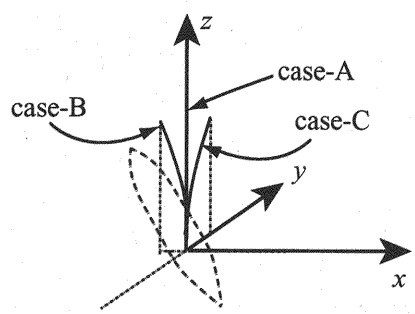

Fig. 17 Coordinate system and basic attitude of numerical model

Fig. 18 shows the predicted snapshots in case-C. From the initial inclined attitude, the propagule model shows some oscillating movements.

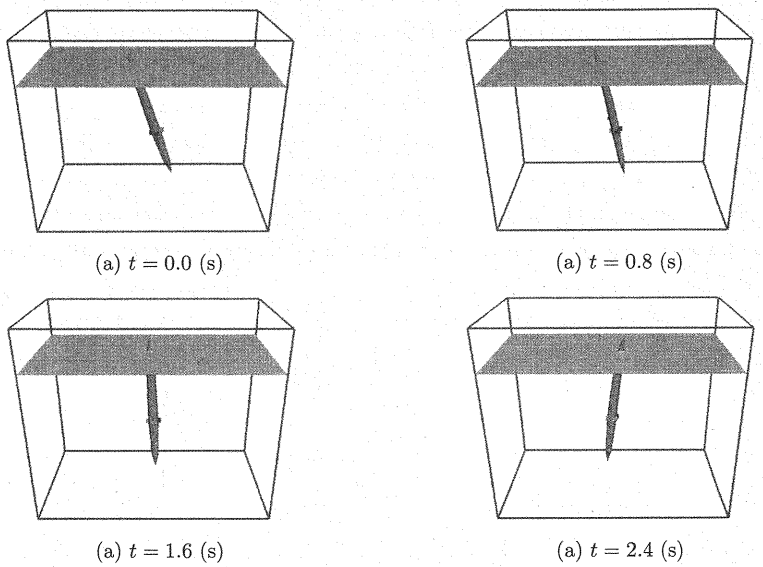

(a) $t = 0.0$ (s)　(a) $t = 0.8$ (s)

(a) $t = 1.6$ (s)　(a) $t = 2.4$ (s)

Fig. 18 Predicted attitudes of propagule model (case-C)

In order to discuss the detailed movements of the propagule model, the positions of the points fixed on the model are tracked in the unsteady computations: the center of gravity G and the reference point Q_1 or Q_2 placed on the surface. The locations of these points on $x-y$ plane are shown in Fig. 19, in which D is the maximum diameter of the propagule model that is given by 15 mm. On the $x-y$ plane, G initially coincides with the origin of the coordinates, while Q_1 and Q_2 are placed on the surface of the propagule model at 70 mm in height from the bottom of the model to detect its swirling motions by tracking the time history of their locations.

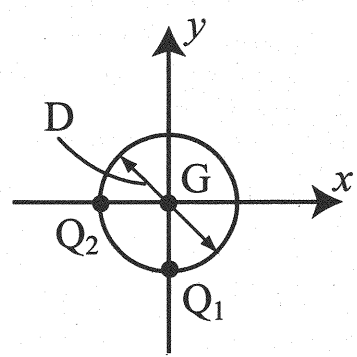

Fig. 19 Locations of G, Q_1 and Q_2 on $x-y$ plane in basic attitude

Fig. 20 shows the trace-lines of G, Q_1 and Q_2 of the moving propagule model on the $x/L-y/L$ plane, where L is 18.8 cm, which is the axial length of the propagule model. The positions of G, Q_1 and Q_2 are tracked from $t = 0$ to 20 sec. In the case-A and B, as shown in Fig. 20, the center of gravity G is almost fixed, meanwhile the

movements of Q_1 are approximately parallel with x axis. This means that the movements of the propagule model in case-A and B are a simple rotational motion around y axis. The movements in case-A and B are caused by the fact that the initial attitude is symmetric with respect to the $x-z$ plane and that the initial small inclination is set only around y axis. In contrast to case-A and B, the trace-lines of Q_2 in Fig. 20 are no longer parallel with the x axis and they show the rotational motions on the $x-y$ plane. Thus, the propagule model in case-C show the swirling motions around z axis, which means the axis of rotational motions does not coincide with the y axis. Conclusively, the present computational methods allows us to predict the complicated motions of the bent propagule model with non-uniform density, which is very similar to the actual mangrove propagules.

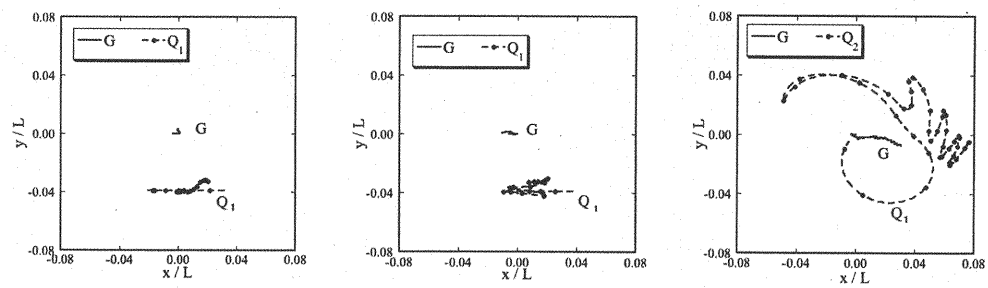

Fig. 20 Trace-lines of G, Q_1 and Q_2 of the moving propagule model

CONCLUSIONS

In this study, a computational method was investigated to predict the motions of a floating object which have non-uniform density in free-surface flows. The floating object is represented by using tetrahedron elements and the density distributions are taken into account by setting the different densities one by one. The floating objects and free-surface flow are dealt with the computational method, MICS, in which the field is taken as a incompressible mixture of gas, liquid and solid phases. The prediction method was applied to the movements of a floating cylinder with non-uniform density. As a result, the stability of the initial attitude, which is related to the density distributions, is accurately calculated with the present method. It was also demonstrated that the present method enables us to predict the free oscillation and the motions in sloshing fluids for the cylinder model. In addition, the computational method was applied to the floating motions of the actual mangrove propagule. It was concluded that the stability of the propagule attitude related to its density distribution, vertical free-oscillations, and rotation and swirling motions caused by the bending of its axis can be reasonably predicted by means of this method.

REFERENCES

1. Komiyama, A., Chimchome, V. and Kongsangchai, J.: *Dispersal patterns of mangrov propagules*, Vol. 57, pp. 27–34, 1992.

2. Ohmatsu, S.: On the oscillation problem of multiple floating bodies in waves, *Papers of National Maritime Research Institute*, Vol. 8, No. 1, 2008.

3. Ushijima, S., Fukutani, A. and Makino, O.: Prediction method for movements with collisions of arbitrarily-shaped objects in 3D free-surface flows, *JSCE Journal*, Vol. 64/II-2, pp. 128–138, 2008.

4. Fukutani, A., Ushijima, S., Makino, O. and Nezu, I.: Applicability of multiphase-flow solver (3D MICS) to movements of floating objects, *J. Applied Mech., JSCE*, Vol. 10, pp. 705–712, 2007.

5. Ushijima, S., Yamada, S., Fujioka, S. and Nezu, I.: Prediction method (3D MICS) for transportation of solid bodies in 3D free-surface flows, *JSCE Journal*, Vol. 810/II-74, pp. 79–89, 2006.

6. Yamamoto, S. and Daiguji, H.: Higher-order-accurate upwind schemes for solving the compressible Euler and Navier-Stokes equations, *Computers Fluids*, Vol. 22, No. 2/3, pp. 259–270, 1993.

7. Ushijima, S. and Nezu, I.: Higher-order implicit (C-ISMAC) method for incompressible flows with collocated grid system, *JSCE Journal*, No. 719/II-61, pp. 21–30, 2002.

8. Ushijima, S. and Okuyama, Y.: Comparison of C-HSMAC and SOLA methods for pressure computation of incompressible fluids, *JSCE Journal*, No. 747/II-65, pp. 197–202, 2003.

APPENDIX-NOTATION

The following symbols are used in this paper:

F_{Ci} = fluid force component acting on a part of solid object in a fluid cell C;

f_i = acceleration component of external force;

g = gravity acceleration;

G = center of gravity;

H = horizontal axis ;

I = moment of inertia ;

l = axial length of cylinder;

p = volume-averaged pressure;

p_0 = hydrostatic pressure;

Q_1 = reference point placed on surface of propagule model;

Q_2 = reference point placed on surface of propagule model;

t = time;

u_i = mass-averaged velocity component in x_i direction;

V_C = volume of fluid cell;

x_i = orthogonal coordinates;

α = volume fraction of solid phase;

γ_i = volume fraction of element i included in a fluid cell C;

$\delta_{i,j}$ = Kronecker's delta;

μ = volume-averaged coefficient of viscosity;

ρ_f = volume-averaged density for gas and liquid phases;

ρ_w = densities of water;

σ_i = density of element i;

(Received Nov, 25, 2009 ; revised Sep, 01, 2010)